Symmetry breaking of in-plane Raman scattering by elliptically polarized light in MoS_2

Teng-De Huang,* Kristan Bryan Simbulan,* Yu-Fan Chiang, Yann-Wen Lan,† and Ting-Hua Lu‡
Department of Physics, National Taiwan Normal University, Taipei 11677, Taiwan

(Received 20 June 2019; revised manuscript received 4 October 2019; published 12 November 2019)

The breaking of the doubly degenerate in-plane lattice vibrations in monolayer, bilayer, and bulk molybdenum disulfide (MoS_2) are oftentimes ignored in the analysis of the material's lattice behaviors due to the lack of variation of polarization for the excitation light. In this work, we have observed variations in the relative intensity of the two most dominant Raman peaks of MoS_2 via polarized micro-Raman spectroscopy using elliptically polarized incident light. The use of elliptically polarized light has demonstrated distinct properties in its incident Raman polarization vector. This gives an additional degree of freedom affecting the relationship between the x (E^1_{2gx}) and y (E^1_{2gy}) components of the material's in-plane lattice vibrations. The different ratio of the magnitudes for the E^1_{2gx} and E^1_{2gy} in the lattice vibrations can be induced by changing the polarization state of the incident light. This work investigates the material's unexplored fundamental phonon property that may enlighten past and future studies involving phonon behaviors.

DOI: 10.1103/PhysRevB.100.195414

I. INTRODUCTION

Layered two-dimensional (2D) transition metal dichalcogenides (TMDs), such as MoS_2, have attracted numerous attention due to their unique physical properties [1–3] and potential applications in optoelectronics [4,5]. The distinct optical properties of 2D materials have been observed via Raman spectroscopy. Raman spectroscopy is a powerful and nondestructive tool that has been used extensively in 2D materials, such as graphene, TMDs, and black phosphorus, to investigate lattice vibrations (phonon mode) [6,7], layer thickness [8,9], stacking sequence [10], crystallographic orientation [11], and interlayer-coupling [12–14] among others. A technique called polarized Raman spectroscopy can further show the material's anisotropic Raman intensity by basically varying the polarization orientation and state of the incident and scattered light. Using incident linearly polarized beams in parallel (XX) or orthogonal (XY) to the scattered light, Zhang *et al.* [15] provided a phonon selection rule that describes the polarization states of the doubly degenerate in-plane (E^1_{2g}) and the nondegenerate out-of-plane (A_{1g}) phonon modes. Their findings clearly demonstrated that, by using an incident linearly polarized light, the A_{1g} and the E^1_{2g} would possess linear and isotropic polarization state, respectively. Meanwhile, another selection rule was reported by Chen *et al.* [16] revealing the Raman modes' effective polarization states arising from an incident circularly polarized light ($\sigma+$ or $\sigma-$). The results apparently show that the E^1_{2g} and the A_{1g} have opposite helicity of circular polarization states, which depends on the helicity of the incident beam. The helicity of the circularly polarized beam is analyzed by the quarter-wave plate (QWP) and analyzer. It is important to note, that the polarized Raman intensity of E^1_{2g} is a superposition of the Raman intensities of its two degenerate states. These two degenerate states of E^1_{2g} describe the material's lattice vibrations along the x and y direction, which can be denoted as E^1_{2gx} and E^1_{2gy}, respectively. Further analysis regarding the relationship of the Raman intensities of E^1_{2gx} and E^1_{2gy}, however, was rarely mentioned.

In this paper, incident linearly and elliptically polarized light were used to induce equal and unequal magnitudes of lattice vibrations, respectively, along the x and the y directions. Equal magnitudes of E^1_{2gx} and E^1_{2gy} were observed when horizontally and vertically polarized light were used; but then, when an elliptically polarized light was applied, the magnitudes of these two components were found to be unequal. Hence, different magnitudes of the components of in-plane lattice vibrations, $I(E^1_{2gx})$ and $I(E^1_{2gy})$, can be observed by changing the polarization state of the incident beam. Accordingly, detailed investigations of the anisotropic behavior of the E^1_{2g} and A_{1g} Raman modes in monolayer, bilayer, and bulk MoS_2 were observed via polarized micro-Raman spectroscopy using different polarized light at tight-focused condition. The experimental polar plot of the Raman intensities and the polarized Raman spectra were analyzed using separate vector representations for the incident and scattered light. Herein, the Raman tensor provides a theoretical description of this intriguing property. All experimental results are in good agreement with the fitted results.

II. CONCEPT AND EXPERIMENTAL SETUP

The Raman intensity for υ phonon mode, $I_s(\upsilon)$, is given by

$$I_s(\upsilon) \propto \sum_{\upsilon} |\hat{E}_s(\theta) R(\upsilon) \hat{E}_i|^2, \tag{1}$$

where

$$\hat{E}_i = \begin{pmatrix} E_x \\ 0 \\ 0 \end{pmatrix} + e^{i\phi} \begin{pmatrix} 0 \\ E_y \\ 0 \end{pmatrix} \quad \text{and} \quad \hat{E}_s(\theta) = (\cos\theta \quad \sin\theta \quad 0)$$

*These authors contributed equally to this work.
†Corresponding author: ywlan@ntnu.edu.tw
‡Corresponding author: thlu@ntnu.edu.tw

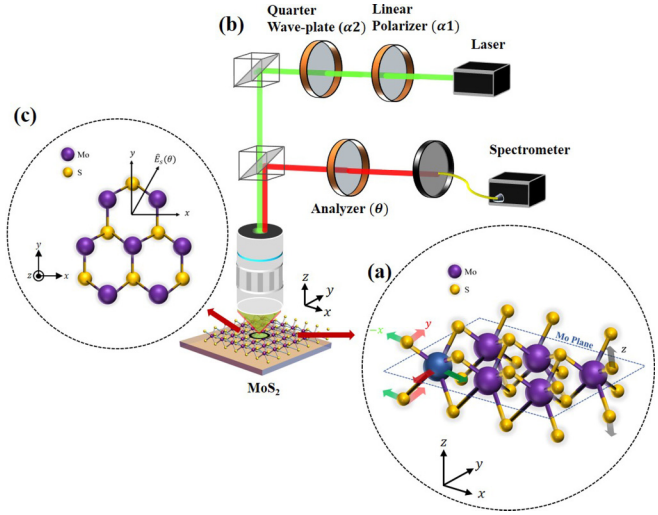

FIG. 1. (a) The phonon mode for MoS_2 presented on side-plane view. The red and green arrows represent the in-plane phonon (E^1_{2g}) mode with two orthogonal (x and y) lattice vibration directions. The grey arrow represents the out of plane phonon (A_{1g}) mode. (b) Micro-Raman spectrometer setup including a linear polarizer, a quarter wave-plate, an analyzer, and a high NA objective lens. The incident polarization state is manipulated by the angles $\alpha 1$ and $\alpha 2$; while the scattered light is analyzed by the angle θ. (c) Schematic diagram of the scattered polarization vector, $\hat{E}_s(\theta)$, presented in the top view.

are the unit polarization vectors of the incident and scattered light, respectively, and $R(\upsilon)$ is the 3×3 Raman tensor. The vector of the incident polarized light ($\hat{E}_i$) is decomposed into x and y components, described, respectively, by E_x and E_y, with a phase difference, ϕ. The polarization state of the incident beam (e.g. linear to elliptical polarization state, or linear to circular polarization state) can be controlled by varying ϕ from 0 to 2π; while its orientation can be characterized by E_x, E_y, and ϕ. The vector of the scattered light is examined via the angles of the analyzer. Some doubly or triply degenerate Raman modes have multiple Raman tensors; therefore, the total Raman intensity is equivalent to the sum of all the Raman intensities each represented by these Raman tensors. The phonon mode is Raman-active if the normal mode belongs to an irreducible representation formed by quadratic basis functions. For monolayer MoS_2, Raman tensors $R(E^1_{2g} : E^1_{2gy}, E^1_{2gx})$ and $R(A_{1g})$ are defined as [15]

$$R\left(E^1_{2g} : E^1_{2gy}, E^1_{2gx}\right): \begin{pmatrix} 0 & d & 0 \\ d & 0 & 0 \\ 0 & 0 & 0 \end{pmatrix}, \begin{pmatrix} d & 0 & 0 \\ 0 & -d & 0 \\ 0 & 0 & 0 \end{pmatrix}$$

and

$$R(A_{1g}): \begin{pmatrix} a & 0 & 0 \\ 0 & a & 0 \\ 0 & 0 & b \end{pmatrix},$$

respectively. Major terms a, d, and b as well as the other zero components in the Raman tensors are related to the symmetry of the material. Figure 1(a) shows the side-plane view of the MoS_2 structure. Here, the E^1_{2g} phonon mode is illustrated as an in-plane vibration, which involves Mo atoms vibrating in directions opposite to that of the S atoms along the surface plane of the material. The x and y components of the E^1_{2g} phonon mode are denoted as E^1_{2gx} and E^1_{2gy}, respectively. For the out-of-plane phonon mode (A_{1g}), the Mo atoms are fixed while the S atoms vibrate perpendicular to, i.e., above and below, the Mo plane. According to a reference [15], an E^1_{2g} mode, due to an incident linearly polarized beam, has an isotropic polarization. With that said, and according to our calculations, the magnitude of the in-plane lattice vibrations should be the same along the x and y directions [$I(E^1_{2gx}) = I(E^1_{2gy})$]. On the other hand, as mentioned in the same reference, the A_{1g} mode should follow the polarization state of the incident beam as it possesses a linear (circular) polarization state when excited by a linearly (circularly) polarized incident light. Elliptically polarized light has rarely been used in polarized Raman spectrum analyses. It can be viewed as having a linear and a circular polarization state component such that the orientation of its major axis is comparable to a linear polarization state, while its apparent helicity is similar to the helicity of the circular polarization state. Thus, elliptically polarized light provides an extra degree of freedom that is useful for investigations using polarized Raman spectroscopy. Polarized Raman spectroscopy utilizing a high numerical aperture (NA) objective lens was used to investigate the intensity of the E^1_{2g} and A_{1g} modes using separate vectors for the incident and the scattered polarization light. The experimental setup is shown in Fig. 1(b). Here, the incident linear, elliptical, and circular laser polarization states are varied according to the relative orientations between the linear polarizer's transmission axis angle ($\alpha 1$) and the QWP's fast-axis angle ($\alpha 2$). An analyzer was also placed prior to the spectrometer entrance, where an angle θ is defined as the analyzer's transmission axis angle. This angle θ was rotated 360° in 24 steps in order to analyze the polarization state of the scattered light. The corresponding scattered polarization vector, $\hat{E}_s(\theta)$, is sketched in the schematic diagram in Fig. 1(c). Note that the positions of the probe laser and the microscope focus are optimized in order to ensure the consistency of the results in every step.

The layered MoS_2 samples were prepared by chemical vapor deposition and were grown onto a 180-nm silicon dioxide on a silicon wafer. Using a micro-Raman spectrometer (Spectra pro 2500i), polarized Raman experiments were performed using a 532-nm (2.33 eV) solid-state laser at room temperature on the monolayer, bilayer and bulk MoS_2 samples. The incident laser passed through a 100x objective lens with a high NA = 0.95 and was operated at a power and spectrometer integration time of 800 μW and 6 s, respectively. Shown in Figs. 2(a) and 2(b) are, respectively, the experimental Raman and photoluminescence (PL) spectra for the monolayer MoS_2 case. The Raman peak separation between the E^1_{2g} and the A_{1g} is around 20 cm^{-1}, denoting a monolayer structure, while the PL graph shows a single high intensity peak representing the A exciton.

III. RESULTS AND DISCUSSION

Figure 2(c) exhibits the Raman spectra of the monolayer MoS_2 sample, using an incident vertically polarized beam,

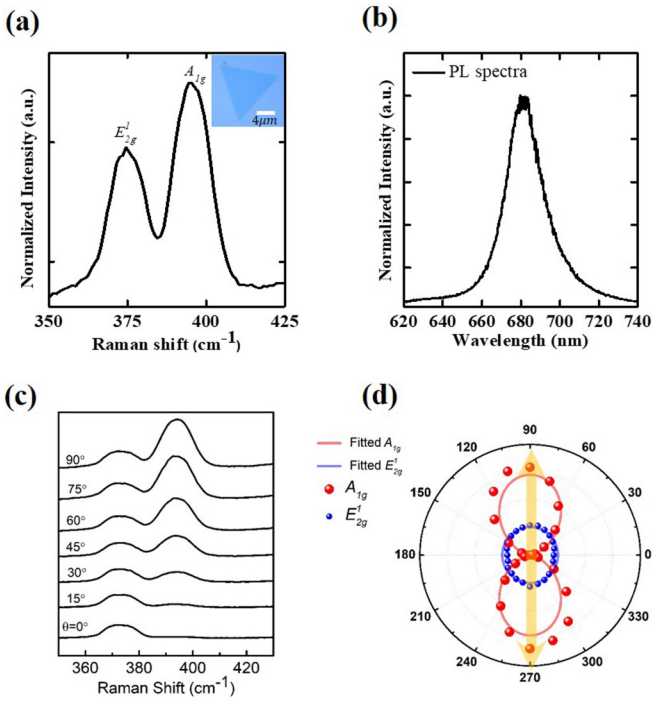

FIG. 2. The (a) Raman and (b) PL spectra of the monolayer MoS_2 sample. The Raman spectra indicate the peak separation between the E^1_{2g} and the A_{1g} modes at around 20 cm^{-1}. Inset in (a) shows the optical microscope image of one of the monolayer triangular MoS_2 samples on Si/SiO_2 substrate used in the experiment. The (c) experimental polarized Raman spectrum and the corresponding (d) polar plot of the Raman intensities resulting from an incident vertical polarization state. The yellow arrow in (d) represents the incident vertical polarization state, and the solid red and blue lines represent the fitted polar plots for the A_{1g} and E^1_{2g}, respectively.

taken at various angles of the analyzer; while Fig. 2(d) shows its corresponding polar plot where the incident beam's vertical polarization state is marked by a yellow arrow. The polar plot of the collective Raman intensity spectra has clearly shown the equivalence (nonequivalence) of the resulting polarization state of A_{1g} (E^1_{2g}) with that of the incident beam since A_{1g} (E^1_{2g}) possessed a vertical (isotropic) polarization. These experimental results were fitted by substituting the parameters of the incident beam's polarization state (i.e., $E_x = 0$, $E_y = 1$ and $\phi = 0$ for vertically polarized incident beam) into Eq. (1). Various incident polarization states, shown in Figs. 3(a)–3(d), were then emitted into the monolayer MoS_2 sample to further observe the ensuing variations of the Raman intensities : these states are, in the order as presented, the horizontal linear polarization state, elliptical polarization state oriented at 45°, vertical polarization state, and elliptical polarization state oriented at 135°. The corresponding Raman intensity polar plots and polarized Raman spectra resulting from these four incident states are accordingly presented in Figs. 3(e)–3(h), Figs. 3(i)–3(l) and Ref. [17]. In cases when the incident beam is horizontally [Figs. 3(a) and 3(e)] and vertically (Figs. 3(c) and 3(g) polarized, the polarization state of A_{1g} simply follows that of the incident beam. These were fitted with the theoretical expressions of the Raman intensity for A_{1g}, which are proportional to the factors $(a\cos\theta)^2$ and $(a\sin\theta)^2$ for the incident horizontally and vertically polarized light, respectively, as derived from Eq. (1) (see Table I). However, the polarization state of the E^1_{2g} modes is isotropic regardless of the orientation (horizontal or vertical) of the incident linearly polarized beam. These were also fitted with the theoretical expressions of the Raman intensity, which are proportional to the factors $m \times (d\cos\theta)^2 + n \times (d\sin\theta)^2$ and $m \times (d\cos\theta)^2 \pm n \times (-d\sin\theta)^2$, for the incident horizontally polarized and vertically polarized light, respectively (see Table I). Here, the parameters m and n are magnitude coefficients of $I(E^1_{2gx})$ and $I(E^1_{2gy})$, which determines the magnitude of the Raman intensities of $I(E^1_{2gx})$ and $I(E^1_{2gy})$. Numerical results indicate an isotropic polarization for E^1_{2g} given that its component's intensities are equal, i.e., $I(E^1_{2gx}) = I(E^1_{2gy})$ and $m = n$.

For an incident elliptically polarized light oriented at 45° ($E_x = 1/\sqrt{2}$, $E_y = 1/\sqrt{2}$ and $\phi = 5.8$), the corresponding polar plot of the Raman intensities for A_{1g} takes the shape of that of the incident beam (elliptical). This is consistent with the recorded behavior of A_{1g} in the case of an incident linear polarization state. Interestingly, the polar plot of Raman intensities of the E^1_{2g} mode also displays an elliptical shape. The magnitude of its components, E^1_{2gx} and E^1_{2gy}, were fitted (see Table I), and it was found that the intensity coefficients m and n have unequal values ($m = 0.7$ and $n = 0.1$). Incident elliptically polarized light oriented at 135° ($E_x = -1/\sqrt{2}$, $E_y = 1/\sqrt{2}$ and $\phi = 5.6$) showed similar results. The polar plots of Raman intensities for the A_{1g} and the E^1_{2g} are also in

TABLE I. The calculated Raman intensity expressions of the E^1_{2g} and A_{1g} for the incident horizontal polarization, vertical polarization, elliptical polarization (oriented at 45°), and elliptical polarization, (oriented at 135°) states, respectively. The operation parameters for the monolayer MoS_2 are shown. Here, m and n are the magnitude coefficients of $I(E^1_{2gx})$ and $I(E^1_{2gy})$, respectively.

	Horizontal linear polarization	Vertical linear polarization	Elliptical polarization orientated at 45°	Elliptical polarization orientated at 135°
Parameters for incident polarization	$E_x = 1,\ E_y = 0,\ \phi = 0$	$E_x = 0,\ E_y = 1,\ \phi = 0$	$E_x = 1/\sqrt{2}, E_y = 1/\sqrt{2},\ \phi = 5.8$	$E_x = -1/\sqrt{2}, E_y = 1/\sqrt{2},\ \phi = 5.6$
E^1_{2g} (Parameters for calculations)	$I(E^1_{2gx}) = m(d\cos\theta)^2$ $I(E^1_{2gy}) = n(d\sin\theta)^2$ $(m = n = 0.3,\ d = 55)$	$I(E^1_{2gx}) = m(d\cos\theta)^2$ $I(E^1_{2gy}) = n(-d\sin\theta)^2$ $(m = n = 0.4,\ d = 55)$	$I(E^1_{2gx}) = m(d\cos\theta - d\cos\phi\sin\theta)^2 + (d\sin\phi\sin\theta)^2$ $I(E^1_{2gy}) = n(d\sin\theta + d\cos\phi\cos\theta)^2 + (d\sin\phi\cos\theta)^2$ $(m = 0.7, n = 0.1,\ d = 55)$	$I(E^1_{2gx}) = m(d\cos\theta + d\cos\phi\sin\theta)^2 + (-d\sin\phi\sin\theta)^2$ $I(E^1_{2gy}) = n(-d\cos\phi\sin\theta + d\sin\theta)^2 + (-d\sin\phi\cos\theta)^2$ $(m = 0.5, n = 0.05,\ d = 55)$
A_{1g}	$I(A_{1g}) = f(a\cos\theta)^2$ $(a = 59, f = 0.9)$	$I(A_{1g}) = f(a\sin\theta)^2$ $(a = 59, f = 1)$	$I(A_{1g}) = f((a\cos\theta + a\cos\phi\sin\theta)^2 + (a\sin\phi sin\theta)^2)$ $(a = 59,\ f = 0.87)$	$I(A_{1g}) = f((a\cos\theta - a\cos\phi\sin\theta)^2 + (-a\sin\phi sin\theta)^2)$ $(a = 59,\ f = 1)$

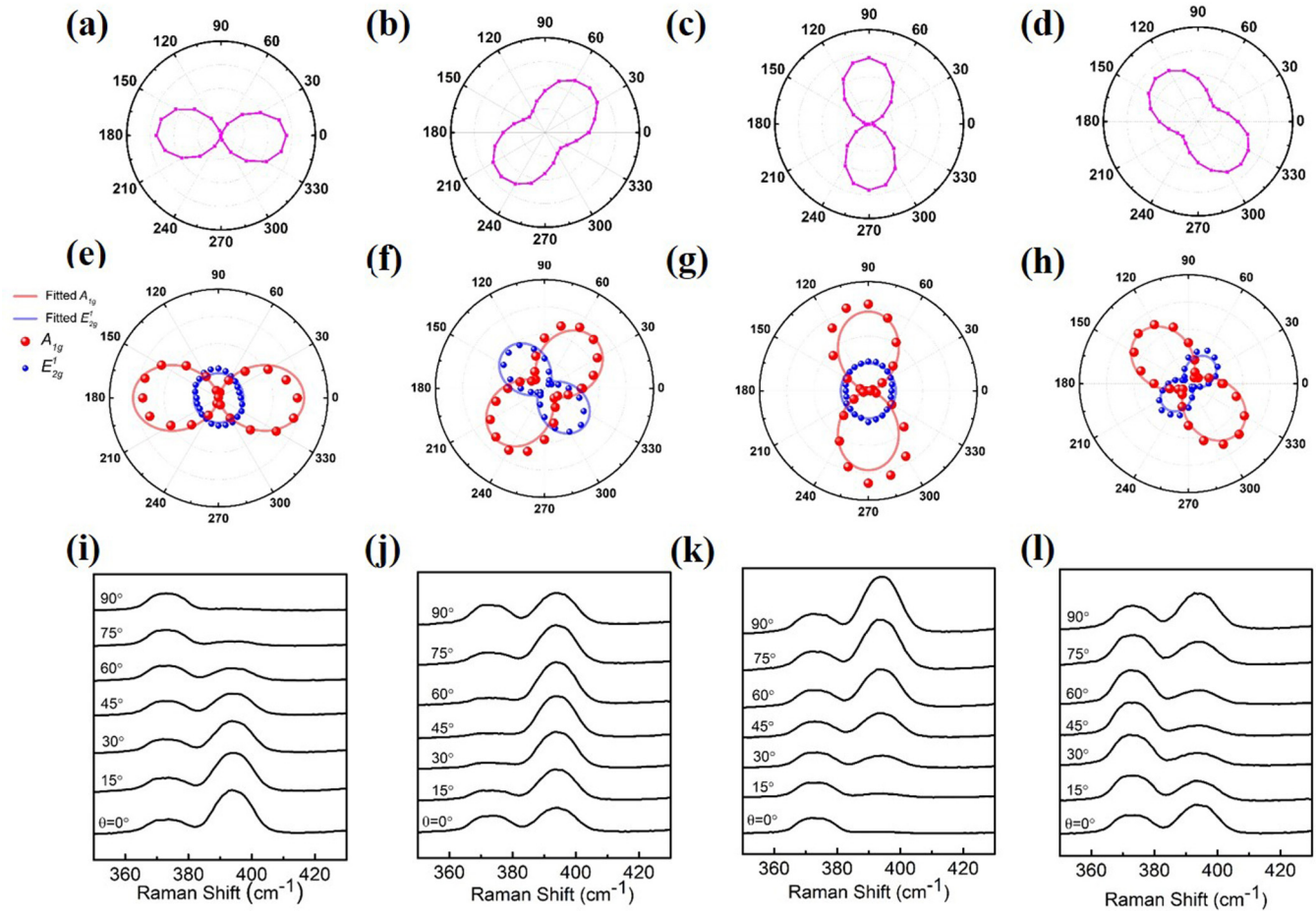

FIG. 3. (a)–(d) Incident polarization states, namely the horizontal linear polarization state, elliptical polarization state oriented at 45°, vertical linear polarization state and elliptical polarization state oriented at 135°, respectively. (e)–(h) Experimental polar plots of Raman intensities, corresponding to the incident polarization states presented in (a)–(d). (i)–(l) Experimental polarized spectra corresponding to (e)–(h). Here, spectra at $\theta = 0^\circ$ to 90° were shown, while the remaining spectra can be found in Ref. [17]. The blue and red solid lines represent the fitted polar plots for the E^1_{2g} and A_{1g} modes, respectively.

the shape of an ellipse with parameters m and n calculated as 0.5 and 0.05, respectively. One may have also noticed that, in Table I, there is a nonequivalence in the values of f among the expressions of the Raman intensities of A_{1g} of the different polarization states. This is caused by the little fluctuation of laser power, which is a deviation of laser stability in the experiment.

The experimental polar plots of the Raman intensities of incident linearly (oriented at 0° and 90°) and elliptically polarized beams (oriented at 15°, 30°, 45°, 60°, 75°, 105°, 120°, 135°, 150°, and 165°) were demonstrated in Ref. [17]. The horizontally, vertically, and elliptically polarized beams are noted as $|H,\rangle$ $|V\rangle$, and $|E\rangle$, respectively. According to the results, the polar plots of E^1_{2g} gradually transformed from isotropic to angle-dependent. Specifically, at $\phi = 0, \pi$ and 2π, which indicates that the incident polarized beam has a linear polarization state, the polar plots of E^1_{2g} show an isotropic behavior; while, at $0 < \phi < 2\pi$ and $\phi \neq \pi$, which results in incident elliptically polarized beams of various eccentricities, the polar plots of E^1_{2g} show an angle-dependent behavior. Based on these results, incident elliptical polarization beams indeed induce unequal Raman intensities for the E^1_{2g} components: E^1_{2gx} and E^1_{2gy}. The fitted results for both the E^1_{2g} (blue solid lines) and the A_{1g} (red solid lines) are also shown in Figs. 3(e)–3(h) and Ref. [17]. The corresponding polarized Raman spectra for the plots in Ref. [17] are exhibited. Details of the calculations were presented in Table I and Ref. [17].

Figures 4(a)–4(h) demonstrate the experimental polar plots of the Raman intensities triggered by incident horizontal, elliptical (oriented at 45°), vertical, and elliptical (oriented at 135°) polarization states for the bilayer and bulk MoS_2, respectively. The results for the bilayer and bulk reveals similar polar plot patterns for both E^1_{2g} and A_{1g} as that of the monolayer variant. The corresponding polarized Raman spectra were also presented in Ref. [17]. The fitted curve has been calculated with Eq. (1) using the Raman tensors for the bilayer and bulk MoS_2 (see Table II). For bulk MoS_2, the Raman tensors (E^1_{2g} and A_{1g}) are identical to that of the monolayer MoS_2. However, for the bilayer MoS_2, while its Raman tensor for the A_{1g} is identical to that of the monolayer variant, its Raman tensor for the E^1_{2g} is unique (see Table II)

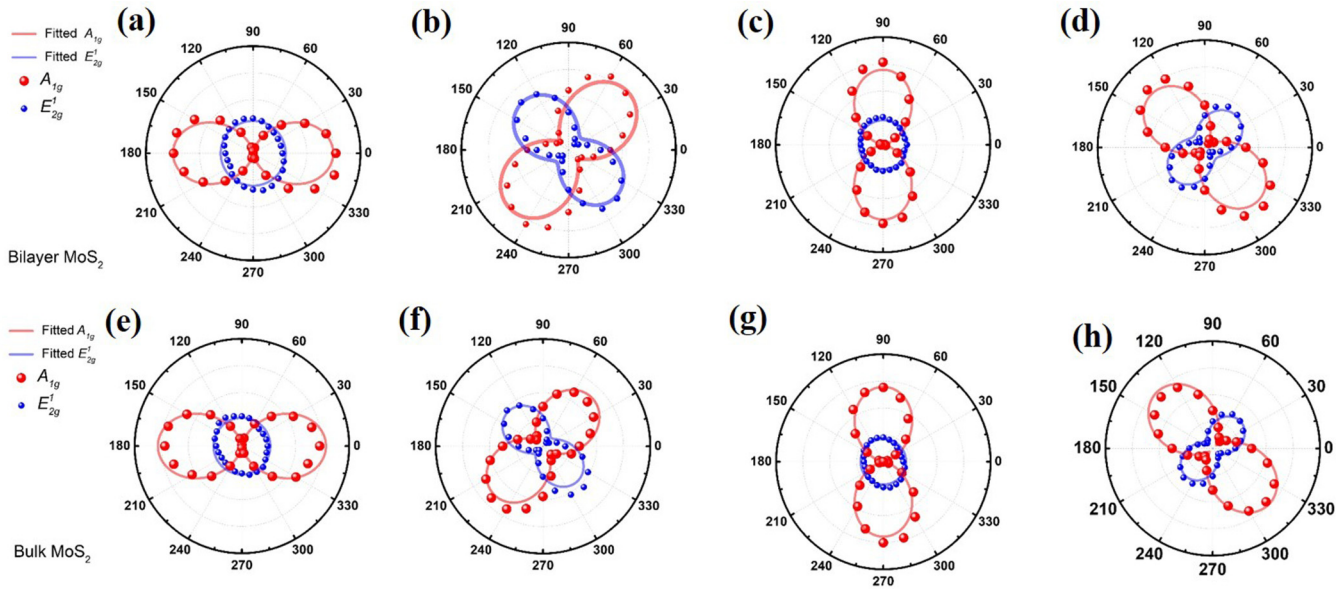

FIG. 4. Experimental polar plots of Raman intensities for the (a)–(d) bilayer MoS_2 and (e)–(h) bulk MoS_2. The polar plots in both cases correspond to the incident polarization states presented in Figs. 3(a)–3(d). The blue and red solid lines represent the calculated polar plots for the E^1_{2g} and A_{1g} modes, respectively.

due to the additional nonzero element brought about by the z-component of incident optical field. As presented in Fig. 4, both bilayer and bulk MoS_2 exhibited Raman intensities with coefficients $m = 1.5$, $n = 0.3$ and $m = 0.7$, $n = 0.05$ when impinged by an incident elliptically polarized light oriented at 45°. Contrasting results, on the other hand, were observed for both materials when impinged with an incident elliptically polarized light oriented at 135° as Raman intensities with $m = 1$ and $n = 0.3$ were recorded for the bilayer, and $m = 0.5$ and $n = 0.1$ were noted for the bulk. Meanwhile, incident horizontally and vertically polarized light induced almost equal Raman intensities along the x and the y directions ($m = n$) also for both materials. Therefore, we can say that incident elliptically polarized beams provide an extra degree of freedom that controls the Raman intensities of the monolayer, bilayer, and bulk MoS_2 along the x and y directions. All the above experimental results are reproducible as they were also observed in the other set of samples and are in good agreement with the fitted results.

IV. CONCLUSION

Incident light with linear and elliptical polarization states were utilized in the polarized Raman spectroscopy analysis of MoS_2. The detailed anisotropic behavior of the E^1_{2g} phonon mode of MoS_2 was also reported. The incident beam's polarization state had been theoretically discussed in terms of its xy components and phase difference, ϕ, in order to demonstrate its transformation to another polarization state by adjusting the orientations of the linear polarizer and the quarter wave plate. The scattered light was analyzed by the polarizer's transmission axis angle. Experimental results revealed that different combinations of Raman intensities, $I(E^1_{2gx})$ and $I(E^1_{2gy})$, were induced by changing the polarization state

TABLE II. The Raman tensors and operation parameters of the E^1_{2g} and A_{1g} for the incident horizontal polarization, vertical polarization, elliptical polarization (oriented at 45°), and elliptical polarization (oriented at 135°) states, respectively, for the bilayer and bulk MoS_2.

	Raman tensor	Horizontal linear polarization	Vertical linear polarization	Elliptical polarization orientated at 45 °	Elliptical polarization orientated at 135 °
E^1_{2g} (Bulk)	$E^1_{2gy} = \begin{pmatrix} 0 & d & 0 \\ d & 0 & 0 \\ 0 & 0 & 0 \end{pmatrix}, E^1_{2gx} = \begin{pmatrix} d & 0 & 0 \\ 0 & -d & 0 \\ 0 & 0 & 0 \end{pmatrix}$	$m = n = 0.35$ $d = 55, \phi = 0$	$m = n = 0.35$ $d = 55, \phi = 0$	$m = 0.7, n = 0.05$ $d = 55, \phi = 5.5$	$m = 0.5, n = 0.1$ $d = 55, \phi = 5.8$
E^1_{2g} (Bilayer)	$E^1_{2gy} = \begin{pmatrix} 0 & -c & -d \\ -c & 0 & 0 \\ -d & 0 & 0 \end{pmatrix}, E^1_{2gx} = \begin{pmatrix} c & 0 & 0 \\ 0 & -c & d \\ 0 & d & 0 \end{pmatrix}$	$m = n = 0.7$ $c = 55, \phi = 0$	$m = n = 0.75$ $c = 55, \phi = 0$	$m = 1.5, n = 0.3$ $c = 55, \phi = 5.8$	$m = 1, n = 0.3$ $c = 55, \phi = 5.8$
A_{1g}	$\begin{pmatrix} a & 0 & 0 \\ 0 & a & 0 \\ 0 & 0 & b \end{pmatrix}$	Bulk: $a = 59, f = 0.9$ Bilayer: $a = 59, f = 1.5$	Bulk : $a = 59, f = 1$ Bilayer : $a = 59, f = 2$	Bulk: $a = 59, f = 0.86$ Bilayer: $a = 59, f = 1.5$	Bulk : $a = 59, f = 0.9$ Bilayer : $a = 59\ f = 1.5$

of the incident beam. Notably, equal magnitudes of E^1_{2gx} and E^1_{2gy} were observed using incident linearly polarized light, while unequal magnitudes of the said components of in-plane vibrations were triggered by incident elliptically polarized beams. This work provides an avenue for exploring phonon properties in TMDs.

ACKNOWLEDGMENTS

The authors thank the Ministry of Science and Technology for their financial support of this research under Contracts No. MOST 107-2112-M-003-012 and No. MOST 105-2112-M-003-016-MY3.

[1] H. Zeng, J. Dai, W. Yao, D. Xiao, and X. Cui, Nat. Nanotechnol. **7**, 490 (2012).

[2] T. Cao, G. Wang, W. Han, H. Ye, C. Zhu, J. Shi, Q. Niu, P. Tan, E. Wang, B. Liu, and J. Feng, Nat. Commun. **3**, 887 (2012).

[3] K. F. Mak, K. He, J. Shan, and T. F. Heinz, Nat. Nanotechnol. **7**, 494 (2012).

[4] K. F. Mak, K. L. McGill, J. Park, and P. L. McEuen, Science **344**, 1489 (2014).

[5] C. M. Torres, Y.-W. Lan, C. Zeng, J.-H. Chen, X. Kou, A. Navabi, J. Tang, M. Montazeri, J. R. Adleman, M. B. Lerner, Y.-L. Zhong, L.-J. Li, C.-D. Chen, and K. L. Wang, Nano Lett. **15**, 7905 (2015).

[6] A. Gupta, G. Chen, P. Joshi, S. Tadigadapa, and P. C. Eklund, Nano Lett. **6**, 2667 (2006).

[7] A. K. Sood, J. Menéndez, M. Cardona, and K. Ploog, Phys. Rev. Lett. **54**, 2111 (1985).

[8] H. Li, Q. Zhang, C. C. R. Yap, B. K. Tay, T. H. T. Edwin, A. Olivier, and D. Baillargeat, Adv. Funct. Mater. **22**, 1385 (2012).

[9] A. Berkdemir, H. R. Gutiérrez, A. R. Botello-Méndez, N. Perea-López, A. L. Elías, C.-I. Chia, B. Wang, V. H. Crespi, F. López-Urías, J.-C. Charlier, H. Terrones, and M. Terrones, Sci. Rep. **3**, 1755 (2013).

[10] C. Cong, T. Yu, K. Sato, J. Shang, R. Saito, G. F. Dresselhaus, and M. S. Dresselhaus, ACS Nano **5**, 8760 (2011).

[11] T. M. G. Mohiuddin, A. Lombardo, R. R. Nair, A. Bonetti, G. Savini, R. Jalil, N. Bonini, D. M. Basko, C. Galiotis, N. Marzari, K. S. Novoselov, A. K. Geim, and A. C. Ferrari, Phys. Rev. B **79**, 205433 (2009).

[12] Y. Wang, Z. Wang, W. Yao, G.-B. Liu, and H. Yu, Phys. Rev. B **95**, 115429 (2017).

[13] L. Ding, M. S. Ukhtary, M. Chubarov, T. H. Choudhury, F. Zhang, R. Yang, A. Zhang, J. A. Fan, M. Terrones, J. M. Redwing, T. Yang, M. Li, R. Saito, and S. Huang, IEEE Trans. Electron Devices **65**, 4059 (2018).

[14] A. A. Puretzky, L. Liang, X. Li, K. Xiao, B. G. Sumpter, V. Meunier, and D. B. Geohegan, ACS Nano **10**, 2736 (2016).

[15] X. Zhang, X.-F. Qiao, W. Shi, J.-B. Wu, D.-S. Jiang, and P.-H. Tan, Chem. Soc. Rev. **44**, 2757 (2015).

[16] S.-Y. Chen, C. Zheng, M. S. Fuhrer, and J. Yan, Nano Lett. **15**, 2526 (2015).

[17] See Supplemental Material at http://link.aps.org/supplemental/10.1103/PhysRevB.100.195414 detailing polarized Raman spectra and intensities for different analyzer angles, incident polarization states and angles, as well as parameters of the incident polarized light and corresponding fitting coefficients for the Raman modes.